Polymer Degradation and Stability 250 (2026) 112140

Contents lists available at ScienceDirect

Polymer Degradation and Stability

journal homepage: www.journals.elsevier.com/polymer-degradation-and-stability

The role of thermo-oxidative degradation on the dynamic behavior of disulfide-based epoxy vitrimers

Niklas Lorenz [a,*], Andreas Klingler [b], William E. Dyer [a], Santiago J. Garcia [a], Baris Kumru [a,c]

[a] Aerospace Structures & Materials Department, Faculty of Aerospace Engineering, Delft University of Technology, 2629 HS Delft, The Netherlands
[b] Leibniz-Institut für Verbundwerkstoffe, RPTU Kaiserslautern-Landau, 67663 Kaiserslautern, Germany
[c] School of Energy Science and Engineering, Vidyasirimedhi Institute of Science and Technology, Rayong 21210, Thailand

ARTICLE INFO

Keywords:
Vitrimer
Disulfide
Epoxy
Degradation

ABSTRACT

Vitrimers are a class of polymer networks that hold promise as recyclable thermosets with self-healing capabilities, enabled by dynamic molecular-level rearrangements. However, achieving the desired network rearrangements usually demands thermal treatments at elevated temperatures substantially above the glass transition temperature T_g while maintaining these harsh conditions for prolonged dwell times. Therefore, the present paper examines the effects of thermo-oxidative degradation on the dynamicity of a disulfide-based epoxy vitrimer. First, comparison with a non-disulfide-containing reference indicates that disulfide bond degradation is the predominant early-stage degradation mechanism. The thermo-oxidative degradation process was described using model-free kinetics fitted to thermogravimetric data, which was subsequently used to selectively control the degradation state of the vitrimer samples as a function of temperature and exposure time. FTIR identified the presence of a highly oxidized carbonyl surface layer, while DMTA confirmed a drop in the primary T_g. Stress-relaxation testing indicates a temporary, favorable effect of decreased crosslink density: increased bond exchange rates, which in turn facilitate shorter dwell times for healing and shape reconfiguration. This manifests as shifts in the initiation of macroscopic flow, reducing the (re)processing temperature regime. In the long run, cleavage of the dynamic S-S crosslinks becomes predominant, adversely compromising the dynamic properties of these systems, as evidenced by incomplete relaxation and reduced macroscopic flow capabilities. These insights into the distinct effects of thermo-oxidative aging provide a critical foundation for evaluating the long-term viability after high-temperature exposure in an oxygen environment and have important implications for designing appropriate (re)processing regimes for disulfide-based epoxy vitrimers.

1. Introduction

Equipping native thermosets with dynamic covalent bonds has the potential to recycle thermoset polymers directly[1] and provides exceptional features like malleability and healing characteristics - previously reserved for thermoplastics [2–5]. An associative exchange mechanism may be introduced in the network via different dynamic chemistries such as transesterification [6], disulfide [7–10], imine [11–13], siloxane [14,15] and urethane [16] exchange - to name a few. This emerging class of materials offers a more sustainable alternative to conventional epoxy resins, enabling recyclability and extended service life through healing [17–20]. With the potential to replace traditional thermosetting materials across various industries, vitrimers could significantly advance sustainable material production, while research into their applications remains in its early stages [3,21]. In particular, the practical application of these materials requires a detailed understanding of their time- and temperature-dependent behavior under harsh conditions, including the elevated temperatures required to activate bond-exchange reactions that enable healing and malleability.

Therefore, thermo-oxidative degradation constitutes a critical consideration, as thermal treatments above the glass transition temperature T_g are usually required to facilitate dynamic bond exchange. Besides, the structural relaxation behavior of vitrimers is chiefly examined at high temperatures to minimize the effect of glassy dynamics. Various authors noted limitations in recyclability and malleability at elevated temperatures [10,22–25] as well as in achieving full recovery of initial performance during the healing and reconsolidation process [25–28], due to interference between the required high-temperature

* Corresponding author.
E-mail address: n.lorenz@tudelft.nl (N. Lorenz).

https://doi.org/10.1016/j.polymdegradstab.2026.112140
Received 20 January 2026; Received in revised form 10 April 2026; Accepted 16 April 2026
Available online 17 April 2026

bond exchange dynamics and thermal degradation.

In general, thermal-oxidative aging in polymers encompasses both physical and chemical aging processes. Physical aging refers to the structural relaxation of a metastable glassy state (i.e., below T_g) towards an equilibrium state [29]. For epoxy resins, reversible physical aging manifests in an increased T_g and storage modulus [30–32]. Contrary, and mostly important with regard to high temperature oxidative aging processes, chemical aging mainly involves changes in the chemical structure of the polymer resulting from side-reactions at elevated temperatures, oxygen, or water exposure, etc. Various studies indicate that thermal-oxidative ageing of epoxy resin primarily involves several chemical reactions, including post-cure [33,34], gradual carbonyl growth in the cross-section [35,36], concentrated in the layer closest to the surface, and chain scission [34,35,37,38], which deteriorates the mechanical properties and darkens the specimens.

During high-temperature exposure (such as 110 - 120 °C) in an oxygen atmosphere, bulk epoxy polymers undergo diffusion-limited oxidation, in which oxygen consumption through chemical reaction occurs faster than it can diffuse through the material, resulting in a gradual carbonyl "skin-core" profile [36,39,40]. These gradual properties give rise to a secondary tan(δ) peak and the reduction in the primary tan(δ) peak (α-relaxation) due to decreased overall mobility by the continuous oxidative crosslinking [34,35,39]. Besides that, the primary T_g decreases due to chain scission [34,37,38] and the storage modulus increases due to internal antiplasticization [37,41] while the failure strain decreases [40].

Besides comprehensive investigations of permanently crosslinked epoxy networks, recent studies have examined the effects of thermo-oxidative [35,42] and hygrothermal aging [35,43] on transesterification-based vitrimers, which are more prone to the hydrolytic impacts than other dynamic systems. Similar to permanently crosslinked networks, a second tan(δ) peak arises and broadens as thermo-oxidation proceeds while tensile strength and failure strains decrease [35]. For more advanced thermo-oxidative degradation, associated with a mass loss of 5.5 %, the compressive strength decreases by up to 27 % [42]. FTIR analysis reveals that thermo-oxidative aging at moderate temperatures (above T_g) is associated with rising transmittance intensities at 1733 cm^{-1} (C=O) and 3360 cm^{-1} (O—H) [42] at the same time increasing the transesterification rate. Still, at ageing temperatures above 200 °C (125 °C above T_g), the 1733 cm^{-1} (C=O) and other peaks gradually disappear, indicating that the backbone chains of the sample thermally decompose. Comparable findings are reported in [35]. However, some absorbance peaks of C—O stretching vibrations from esters (1256 and 1072 cm^{-1}) and C–H bending modes of aromatic rings (1006 and 788 cm^{-1}) remain, which may indicate that the backbone chains were not completely deteriorated, thanks to lower temperatures. Besides that, the decrease in C–H absorbance without a corresponding increase in C = O peaks indicates that oxidative chain scission, rather than carbonyl formation, dominated the degradation pathway [42].

Moreover, some literature investigates thermo-oxidative degradation and degradation kinetics based on mass loss recorded during ramped thermogravimetric analysis [44–46]. For disulfide-based vitrimers, studies reveal that the initial mass loss can be attributed to the formation of volatile SO_2 from the cleavage and oxidation of disulfide bonds within the aromatic disulfide hardener [44]. The thermal stability of aromatic disulfide bonds is assessed in [47]. The authors conclude that samples must be processed for short times (e.g., 10 min) and at temperatures below 210 °C to prevent significant degradation, as evidenced by nuclear magnetic resonance analysis combined with chemometric tools and deterioration of apparent T_g. Extended thermal cycling (30 ramped cycles from 30 to 100 °C) imposed to a vitrimer network bearing disulfide bonds reveals reduced healing efficiency which the authors attributed to partial thermal degradation [48]. Further research on the thermal decomposition of disulfides spans both small organic molecules [49,50] and complex polymer systems [51–54], generally highlighting a mechanism based on free-radical formation followed by the evolution of volatile sulfur species. In polyurethanes, the onset of degradation tends to decrease with increasing disulfide concentration, with values above 300 °C [53], and 270 °C are reported for non-crosslinked networks [54]. For disulfide-based polyesters, during polymer synthesis, discoloration in the final material suggests S-S bond side reactions at 220 °C [52]. The synthesis of polyolefins with disulfide units incorporated into the main chain is reported to yield thermally processable materials, with decomposition temperatures (above 300 °C) significantly higher than their melting points, allowing for stable manufacturing before degradation[51]. Besides, the sulfur bonds in polymeric networks are susceptible to thermal oxidation [55], therefore suggesting that the vitrimer network can be impacted even before bond cleavage occurs.

In summary, the literature highlights that disulfide bonds impose intrinsic limitations in thermo-oxidative stability, which may critically influence vitrimer (re)processing and durability. Yet, their impact on dynamic network behavior remains insufficiently understood. Therefore, elucidating how thermo-oxidative degradation influences the processing window and long-term dynamic performance of vitrimers is essential for their practical application and is addressed in this work. In addition to thermochemical degradation, thermal degradation is examined separately first. Owing to its practical relevance, the primary analysis focuses on degradation in an oxygen atmosphere, representative of typical conditions encountered during reprocessing, healing, and stress-relaxation testing.

In detail, we study the impact of thermo-oxidative degradation on glass transition, stress relaxation, and the macroscopic flow behavior. First, model-free kinetics are applied to derive a kinetic description of the thermo-oxidative degradation process. Based on that, temperature degradation programs were implemented to obtain polymer specimens with tailored degradation states for further analysis by dynamic thermomechanical analysis and stress relaxation testing. This approach enables us to relate the apparent thermo-oxidative degradation state to changes in dynamic macroscopic properties. Consequently, the findings clarify how thermo-oxidative degradation affects the dynamic properties of a disulfide-based epoxy vitrimer during prolonged dwell periods at the elevated temperatures required to activate dynamic bond-exchange reactions that impart self-healing capability and malleability.

2. Materials and methods

2.1. Materials

1,4-butanediol diglycidyl ether (BDE, epoxy equivalent weight of 101.125 g/eq.), 4,4′-ethylenedianiline (EDA, amine equivalent weight of 53.073 g/eq) and 4-aminophenyl disulfide (4-AFD, amine equivalent weight of 62.093 g/eq.) are purchased from Sigma-Aldrich Corp., Netherlands, and Molekula Ltd., UK, respectively [56]. Small batches of reactive mixtures are prepared according to the procedure described in the supplementary information, maintaining an off-stoichiometric NH_2/epoxy ratio of 1.2 for the dynamic system (BDE-4-AFD) and a stochiometric ratio for the non-dynamic reference (BDE-EDA). An off-stoichiometric ratio is intentionally chosen to enable complete stress relaxation, as reported in [9], since stoichiometric mixtures may undergo epoxy group homopolymerization, yielding non-dynamic crosslinks and thus preventing complete relaxation [57].

2.2. Characterization

Thermogravimetric analysis (TGA) was performed using a TGA DSC3+ from Mettler-Toledo Inc., Switzerland. All measurements were performed in air or nitrogen at a flow rate of 30 mL/min. Samples with masses of 10 ± 1.5 mg were degraded over the temperature range of 120 to 650 °C at heating rates of 1.25, 2.5, 5, 7, 10, and 12.5 K/min. To avoid deviations between the imposed and apparent sample temperatures,

higher heating rates were not considered. For reproductive conditioning and moisture release, samples were dwelled at 120 °C for 120 min immediately before starting the ramped heating step. Additionally, mass loss during isothermal dwellings at 120 to 240 °C is monitored in an air atmosphere for 180 min.

For dynamic mechanical thermal analysis (DMTA) using the RSA-G2 device from TA Instruments (USA), neat resin films were prepared according to the methods described in the supplementary information (cf. Section S1). Subsequently, samples are selectively degraded in a convection oven by imposing the temperature programs described in Table 1. DMTA was used to characterize (i) the storage and loss modulus temperature-dependence for polymers with different degradation states, and (ii) describe the bond exchange kinetics of the disulfide bonds by employing stress relaxation tests in the rubbery regime. All DMTA testing was performed utilizing a film tensile clamp. For temperature sweeps in (i), rectangular specimens (6 × 0.8 × 30 mm³) were heated under air with 3 K/min from 30 to 130 °C with a static tensile force of 0.1 N, and a modulation frequency of 1 Hz while applying a dynamic displacement of 0.01 % (in the linear viscoelastic region). For (ii), the samples were exposed to isothermal stress relaxation tests under an air atmosphere, applying an instantaneous stress of 1 % within 0.1 s at temperatures ranging from 140 to 200 °C within 20 °C increments.

Thermomechanical analysis (TMA, TMA 4000 from PerkinElmer Corp., USA) was used to investigate the macroscopic flow, i.e., the shape change behavior of the different specimens, depending on their degradation state. First, heating rates of 20 K/min (representative for polymer processing) were used to heat the specimens to 190 °C, followed by 12 min at 190 °C (to eliminate any metastable material states imposed by the manufacturing process [58] and rejuvenate any consequence of physical ageing), and finally cooled at 1 K/min in a nitrogen atmosphere until room temperature. A nominal force of 0.1 N maintained the contact of cylindrical specimens (with a diameter of 4 mm and a thickness of 1.9 ± 0.05 mm) and the glass probe (4 mm diameter) during the measurement. Previously, it was shown that the flow behavior of vitrimers is affected by the temperature rates and the applied stress [59,60]. Nevertheless, following Klingler et al. [58], using a minimal tracking force during cooling-controlled TMA can be used to show when the temperature-induced and degradation-controlled flowability of the differently degraded vitrimers disappears. Note that we purposely omit a reference to a vitrimer transition temperature and instead refer to the complex experimental situation surrounding such a transition temperature [58,61,62]. The top and bottom sample surfaces of the specimens molded in the metal tool are smooth and plain, so no additional surface finishing was required. Before testing, thin aluminum films are placed on the bottom and top surfaces of the resin specimen to prevent sticky samples from adhering to the testing device and to reduce friction in the radial direction [59]. The thermal expansion of the aluminum film does not significantly contribute to the measured overall thermal expansion (Figure S11), and the accompanying absolute error in the measured total strain is located below 1 %.

To monitor changes in surface functionality during degradation, degraded rods were subjected to ATR-FTIR (Spectrum 100 FTIR Spectrometer, PerkinElmer, Inc., US), and spectra were recorded over the 600–4000 cm^{-1} range with a resolution of 1 cm^{-1}. The recorded spectra were baseline-corrected using PerkinElmer Spectrum software and normalized to the peak at 1510 cm^{-1} (aromatic C—C stretch). Overlapping peaks in distinct regions of the spectra were deconvoluted using a multiple-Gaussian peak function in MATLAB (MathWorks Inc., USA) to support a more detailed analysis.

Table 1
Temperature programs to selectively degrade the specimens.

#	Degradation [%]	Temperature [°C]	Time [s]
0	0		
1	0.1	190	1237
2	0.2	200	1184
3	0.5	213	1193
4	1	220	1504
5	1.5	229	1165
6	2	225	2296
7	2.5	230	2160
8	3	230	2725
9	4	230	3366

3. Results and discussion

First, the degradation kinetics derived from TGA data are examined, providing the foundation for designing temperature programs to degrade specimens at well-controlled levels of degradation. Subsequent DMTA and TMA were used to evaluate the effect of the degradation degree on the thermomechanical material response, the bond exchange kinetics, and the initiation of macroscopic flow.

3.1. Modeling thermal degradation

Kinetic modeling of thermogravimetric degradation represents an essential step toward correlating arbitrary temperature histories of the material with the resulting degradation state. Therefore, the recorded mass loss during TGA at multiple heating rates is used to model the degradation of the dynamic and non-dynamic polymer matrix using model-free kinetics [45,63]. TGA measures the mass change of the sample over time and temperature during heating in air and nitrogen atmospheres (Fig. 1a, Figure S2). The actual weight $m(t)$ is then translated into conversion $\alpha(t)$, representing the apparent degradation value:

$$\alpha(t) = \frac{m_0 - m(t)}{m_\infty - m_0}, \tag{1}$$

while m_0 and m_∞ represent the initial and final mass of the sample (at 650 °C), respectively. By introducing a generalized kinetic equation, the degradation rate $\frac{d\alpha}{dt}$ can be described by a temperature-dependent rate constant $k(T)$ and a mass-dependent reaction model $f(\alpha)$ [64]:

$$\frac{d\alpha}{dt} = k(T)f(\alpha). \tag{2}$$

While assuming that $k(T)$ follows Arrhenius law and applying a constant heating rate β, the degradation rate $\frac{d\alpha}{dt}$ can be numerically calculated from the temperature and conversion data according to:

$$\beta\frac{d\alpha}{dT} = \exp\left(\frac{-E}{RT}\right)f(\alpha), \tag{3}$$

where $\beta = \frac{dT}{dt}$, represents the heating rate, E the apparent activation energy of the degradation process, and R the universal gas constant. The mathematical manipulation of Equation (3) enables the determination of kinetic triples (E, A and $f(\alpha)$) utilizing the degradation data obtained from multiple heating rates. Isoconversional methods can provide meaningful insights into mechanistic analysis, detecting governing degradation mechanisms [65,66]. The isoconversional principle states that the degradation rate $\frac{d\alpha}{dt}$ at a certain isoconversional value α ($0 \leq \alpha \leq 1$) is solely a function of temperature [67,68]:

$$\left[\frac{\partial \ln\left(\frac{d\alpha}{dt}\right)}{\partial T^{-1}}\right]_\alpha = -\frac{E_\alpha}{R}, \tag{4}$$

whereas E_α is the apparent activation energy for a conversion α, and R is the universal gas constant. Based on Eq. (4) a model-free value of the apparent activation energy can be estimated for each α value. Within the present work, we utilize the differential Friedman's method [69]:

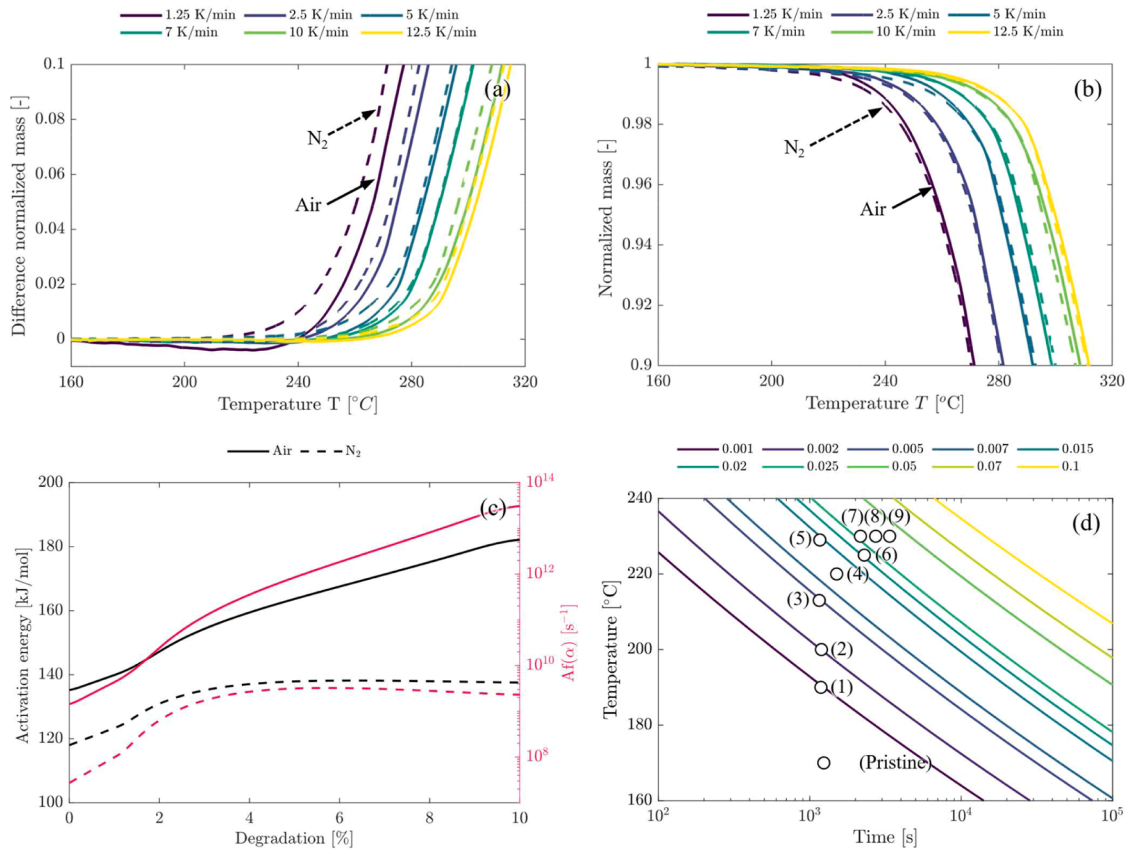

Fig. 1. Difference in normalized mass ($m_{BDE-EDA}(T) - m_{BDE-4AFD}(T)$) of non-dynamic (BDE-EDA) and vitrimeric system (BDE-4AFD) in air (solid) and in nitrogen atmosphere (dashed) at different heating rates (a). Comparison of vitrimer weight loss in air (solid) and nitrogen (dashed) atmosphere at different heating rates (b). Activation energies and pre-exponential factors during the thermal degradation in air and nitrogen atmosphere (c). Time-temperature-transformation diagram for the thermal degradation in an air atmosphere (d). Circles indicate selectively degraded states, as shown in Table 1.

$$\ln\left(\frac{d\alpha}{dt}\right)_{\alpha,i} = ln[A_\alpha f(\alpha)] - \frac{E_\alpha}{RT_{\alpha,i}}. \tag{5}$$

Applying this method requires knowledge of the degradation rate $\left(\frac{d\alpha}{dt}\right)_{\alpha,i}$ and the corresponding temperature $T_{\alpha,i}$ for a specific extent of conversion α across i temperature programs used [65]. The E_α values are calculated for α ranging from 0.01 - 0.1 within steps of 0.001 yielding 91 sampled values, considering advanced values above 0.1 not of practical relevance for degradation during the processing-specific temperature treatments.

The six temperature programs include heating with heating rates β_i of 1.25, 2.5, 5, 7, 10 and 12.5 K/min. For each β_i, the $\left(\frac{d\alpha}{dt}\right)_{\alpha,i}$ and $T_{\alpha,i}$ values are derived. As the term $ln[A_\alpha f(\alpha)]$ remains constant for a particular value of α, the left-hand side of Equation (5) depends linearly on the reciprocal temperature. Taking advantage of this linear correlation, the effective E_α can be calculated from the slope while $A_\alpha f(\alpha)$ represents the y-intercept, respectively (Figure S3).

To solve this kinetic problem for an arbitrary temperature program $T(t)$, the approach suggested *by Farjas and Roura* can be applied [70] to discretize the dependence of temperature on time into constant time intervals, Δt, so that $t_k = k\,\Delta t$, where k is a natural number and $T_k = T(t_k)$. The method is derived directly from Eq. (2) by replacing the differentials by increments yielding:

$$\alpha_{k+1} = \alpha_k + A_{\alpha,k} f(\alpha_k) \exp\left(\frac{-E_{\alpha,k}}{RT_k}\right)\Delta t. \tag{6}$$

Distinct pairs of activation energy and pre-exponential factors with defined Δt of 0.1 s. $E_{\alpha,k}$ and $A_{\alpha,k} f(\alpha_k)$ in Eq. (6) are interpolated from discrete sets of $E_{\alpha,j}$ and $A_{\alpha,j} f(\alpha_j)$ [63] with j ranging from 0 to 1000 and covering an α-range of 0.0 - 0.10. Following the methodology outlined, kinetic evolutions through direct time integration of the transformation rates are employed to predict the kinetics of decomposition under arbitrary temperature profiles, showing good agreements for non-isothermal (Figure S4) and isothermal (Figure S5) conditions with mean average errors of 0.28 % and 0.45 % in the relevant regime (covering times up to 60 min and maximum degradation of 10 %).

Fig. 1a shows differences in the normalized mass loss of non-dynamic (BDE-EDA) and vitrimeric system (BDE-4AFD) in air and nitrogen atmosphere for different heating rates. The consistently positive values indicate premature degradation of the dynamic system, suggesting preferential degradation of the disulfide crosslinks. The observations are consistent with those of *Sanchez-Rodriguez* et al. [44], which identify disulfide bonds in the same aromatic hardener as the predominant early-stage degradation mechanism. Using TGA-FTIR coupling, the authors state that SO_2 formation is the predominant degradation mechanism during early-stage thermal degradation. Based on these findings, we propose that the initial mass loss in the dynamic network results from the cleavage of disulfide bonds and the release of volatile SO_2, thereby constraining the dynamic capacity of the system. Fig. 1b compares the mass loss of the vitrimer for different heating rates in an air and nitrogen atmosphere. Notably, a shift in degradation towards higher temperatures with increasing heating rate is observed during the early stages of thermal exposure in air, attributed to oxygen uptake associated with the oxidation of disulfide linkages. In this regime, the formation of oxidized sulfur species may add oxygen to the network, while higher temperatures and longer residence times cause S-S and C-S bond cleavage in the

later stage, releasing SO_2 as shown in [44], thereby making mass loss dominate. The overall effect is reflected in a transient shift in mass loss, implying the chemical incorporation of oxygen into the polymer backbone.

The derived activation energies for the thermogravimetric degradation of the disulfide vitrimer, shown in Fig. 1c, range from 120–180 kJ/mol and are in the range of disulfide vitrimers in the literature [45], and far below transesterification vitrimers with average values of 260 kJ/mol [46], showing the relevance of premature degradation of disulfide crosslinks. The derived activation energies and preexponential factors, also for the BDE-EDA formulation, are provided in Figure S3a and Figure S3b. Strong correlations were observed, as evidenced by high correlation coefficients.

As a consequence, while samples exposed to air show a continuous increase in the apparent activation energies E_a, the E_a in a nitrogen atmosphere (dashed black line in Fig. 1c) remains close to constant after 2 % degradation. The not strictly constant E_a values in the 0 – 2 % conversion range may be attributable to high noise sensitivity, particularly at low conversions [71]. These observations suggest that continuous oxidation of the S-S bond, accompanied by the conversion of linear S-S bonds to the bent S-O or SO_2 bond architecture, may increase network density. Such densification could manifest in increased E_a values by network constraints and reduced chain mobility. Consequently, as oxidation proceeds, the degradation mechanism transitions from low-energy S-S scission to S-O or even C-S bond cleavage in a more dense network, which is associated with higher bond dissociation energies. Similar steady increase in E_a has been reported for thermo-oxidative degradation of densely crosslinked natural rubber [55].

Based on the derived kinetic models, dwelling cycles provided in Table 1 are designed to selectively degrade specimens according to the protocol described in section S3, resulting in thermogravimetric degradation of 0–4 %. Besides, a time-temperature transformation diagram for the thermo-oxidative degradation of the investigated vitrimer is derived in Fig. 1d. We deliberately selected degradation in an oxygen atmosphere, as this represents the widespread processing boundaries for reprocessing, healing, or stress-relaxation testing. Indeed, the chosen increments (cf. Table 1) are small compared to the reported average model errors of 0.22 - 0.46 %. However, the model consistently underestimates thermogravimetric degradation under isothermal conditions (cf. Figure S5), indicating a potential error that manifests as a uniform shift within the test space and suggesting measurable differences in the comparatively larger interval of 0 – 4 %.

The temperature-time domain is chosen to maintain a constant degradation rate (close to 20 min) up to 1.5 % and to avoid temperatures above 230 °C, which could lead to direct carbon combustion and other unwanted high-temperature conversions.

3.2. *Effect of thermo-oxidative degradation on the dynamic glass transition temperature*

Results of the oscillating temperature sweeps are shown in Fig. 2a. First, it becomes apparent that the glass transition temperature, determined by the loss modulus E'' peak, decreases with increasing degree of degradation, due to oxidation-induced chain scission [34,37,40]. Notably, T_g deterioration seems more pronounced at earlier degradation stages, which may be associated with the premature irreversible breakage of the dynamic S-S crosslinks as implied by the directed comparison of the dynamic network and non-dynamic equivalent (cf. Fig. 1a). Fig. 2b shows the stretched exponential decay of the glass transition temperature with degradation. Indeed, the E'' peak, associated with maximum dissipation energy represents the most appropriate criterion to capture the glass transition temperature enforced by local segmental motion [72,73]. However, we analyze the *tan* δ appearance beyond that, as it reflects the superimposed contributions of both, E' and E'', which exaggerate heterogeneity and make it more sensitive to structural gradients.

Interestingly, analyzing the *tan* δ peak reveals that continued oxidation manifests in a second peak (Figure S6), while retaining a distinctive primary peak in all instances (cf. Figure S7a). Therefore, decreased *tan* δ peak intensities directly relate to a reduced extent of motion associated with the glass transition (due to a more rigid oxidative layer). Yet it should be stressed that DMA probes continuum properties, preventing the derivation of any spatial information from the test sample. Conversely, with increasing degradation, the width of the tan δ peak broadens, indicating a more inhomogeneous network structure [74] and a higher degree of microstructural heterogeneity [75,76], possibly due to thicker oxidized surface-near layers (by prolonged aging times). Above 0.5 % degradation, a secondary peak starts to develop and consequently shifts to higher temperatures while decreasing in intensity (cf. Figure S6f and Figure S7a). This secondary peak formation is typical of epoxy-amine networks subjected to thermo-oxidative aging, in which a "skin-core" structure arises [34,39,77] due to diffusion-limited oxidation (DLO). Literature reports values of 0.2–0.25 mm at 110 °C [36,78] and 0.2 mm at 150 °C [41], with the oxidized layer thickness expected to decrease with increasing exposure temperature [79,80]. Therefore, for a sample thickness of 0.8 mm, the specimens are expected to retain an unaged core region and exhibit an overall heterogeneity within the cross-section. The change in surface color, as shown in Figure S13, indicates surface oxidation.

To provide further evidence for oxidation, Fig. 3a and Fig. 3b show the FTIR spectra for various thermo-oxidative aging stages. One can identify emerging peaks at around 1655 cm^{-1} and 1715 cm^{-1}, indicating the formation of amide and other carbonyls from oxidative crosslinking [39,81]. The latter is presumed to originate from various

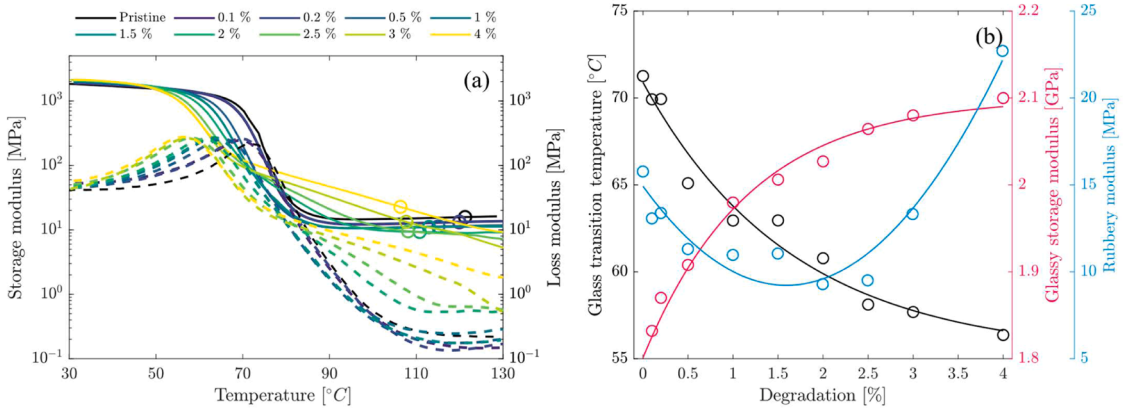

Fig. 2. Temperature-dependent storage (solid) and loss (dashed) modulus for the different degradation states (a). Circles indicate rubbery plateau values at $T_g + 50$ °C to calculate crosslinking density. Development of the glass transition temperature and the glassy and rubbery storage modulus with degradation (b).

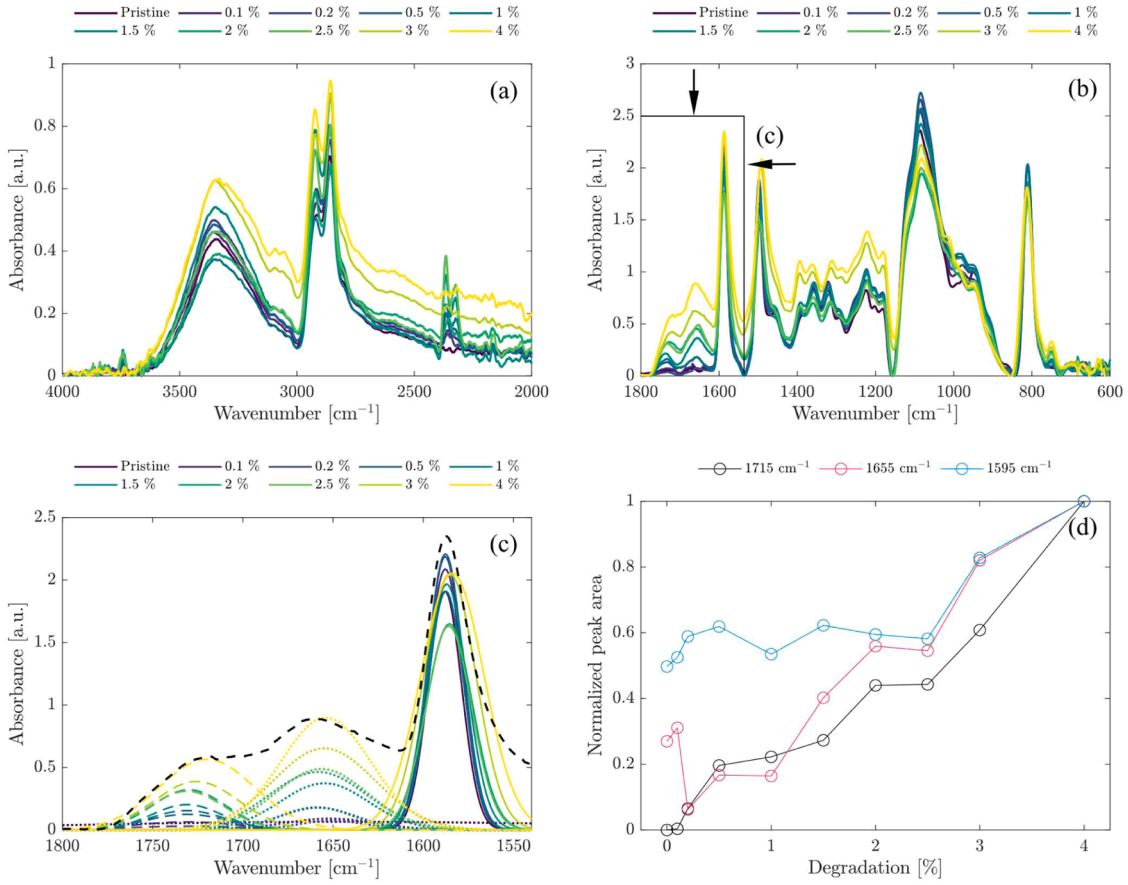

Fig. 3. Higher wavenumbers above 2000 cm^{-1} (a) and lower wavenumbers below 1800 cm^{-1} (b) of FTIR spectra with normalized absorbance for pristine and aged epoxy vitrimer. Deconvoluted 1715 cm^{-1}, 1655 cm$^{-1,}$ and 1595 cm^{-1} peaks indicate carbonyl formation from oxidative crosslinking. The black curve represents the curve enveloping the measurement data. (c). Normalized peak area of 1715 cm^{-1}, 1655 cm$^{-1,}$ and 1595 cm^{-1} peaks (d).

C=O-containing species, such as imides, carboxylic acids, and esters [81,82]. Specific reaction pathways for the oxidation of epoxy-amine systems and oxidation products are proposed in [81,82]. The authors report that the methyl groups of the hardener are more sensitive to oxidation, leading to the co-oxidation of several methylene groups in the α-position of nitrogen atoms. A clear correlation between the consumption of methylene groups in hardener moieties and the formation of amide groups suggests that the mechanism is representative. However, a more detailed analysis of the reaction mechanisms underlying thermo-oxidative degradation is beyond the scope of the present study.

Besides that, the pre-existing peak at 1595 cm^{-1} associated with the C=C stretching broadens, suggesting that the moieties surrounding the aromatic hardener have undergone oxidation and/or further crosslinking, creating a chemically heterogeneous environment around the aromatic rings and leading to multiple overlapping aromatic C=C vibrational contributions in varied local environments. The peaks in that distinct region (1800 - 1500 cm^{-1}) were deconvoluted (Fig. 3c), and the normalized peak area as a semi-quantitative indicator was calculated to outline the continuous increase in absorbance in the amide and carbonyl region (Fig. 3d). Besides that, the 3250 cm^{-1} band broadens (cf. Figure S9), indicating an increase in the O—H stretching vibration of hydroxyl groups (3200 - 3700 cm^{-1}). Therefore, the enhanced O—H stretching vibration of hydroxyl groups, together with the emergence of a new peak in the carbonyl region at 1715 cm^{-1}, indicates the formation of carboxylic acid groups on the material surface [39]. It can be concluded that the surface chemical structure of the epoxy vitrimer changes during thermo-oxidative aging, very similarly to that of an epoxy resin, particularly in the formation of amide and other carbonyl groups as reported in literature [34,39,81,82]. However, accurate estimation of bond formation or dissociation, and of changes explicitly associated with the presence of dynamic disulfide bonds, may require additional characterization beyond the scope of the present study.

While the literature reports a rising second-peak tan δ intensity and a shift to higher temperatures [46,50], the peak intensity decreases significantly in the present case (cf. Figure S7). Again, we assume that the relatively weak dynamic disulfide crosslinks are responsible. Although the peak shifts to higher temperatures as the concentration of oxidative crosslinks in the outer oxidized layer increases, oxidized bonds may simultaneously be broken, leading to a decrease in peak intensity.

Besides, the storage modulus at ambient temperature, i.e., in the glassy state, increases according to a saturating exponential function (cf. Figure S7b) and shows a negative linear correlation with the alpha relaxation behavior (Fig. 4). This counterintuitive behavior is worth noting. Surface near-generation of polar species by thermo-oxidative degradation tends to increase the overall cohesive energy density (or stronger intermolecular interactions causing antiplasticization [37,40,41]). Since cohesive energy density is directly proportional to the glassy modulus [83], an increase in cohesive energy density would enforce a stiffer material behavior. Simultaneously, the crosslinking density decreases (as indicated by dropping rubbery modulus values) while the network density simultaneously decreases, resulting in a reduced T_g. Besides thermo-oxidative degradation, such behaviour may also be attributed to a shift in the amine/epoxy ratio r (1.2 in our case) [84], but it seems to be of subordinate importance in our case (cf. Figure S8) and is kept constant.

Indeed, degraded specimens exhibit a decreased network density ν_e (based on an evaluation of the rubbery module at T_g + 50 °C, cf. Table S1) so that we could expect a more flexible network that can be

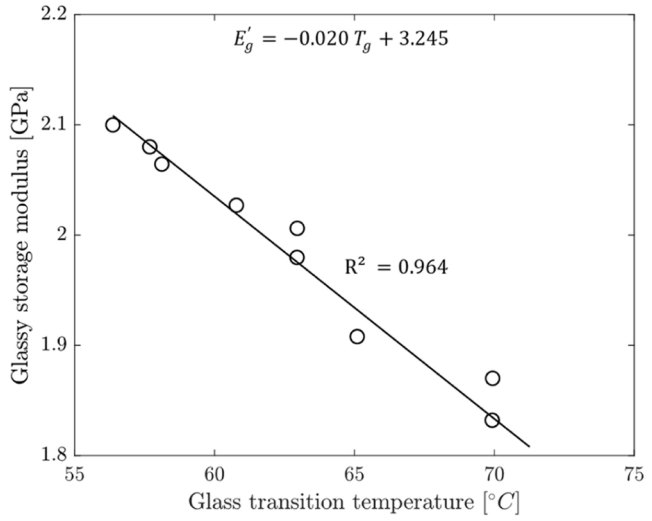

Fig. 4. Correlation of glass transition temperature and ambient temperature glassy storage modulus.

beneficial for more rapid associative bond exchange and associated malleability. In other words, a balance between network degradation by dynamic bond cleavage and oxidative deactivation of these bonds may determine the residual fluidity imparted by the remaining dynamic bonds. Still, caution is required when analyzing the rubbery plateau values of the 3–4 % degraded specimens, with forces reaching final values of 40–60 mN, which are therefore closely located within the standard force tolerances of 10 mN [85]. Further, these degraded samples have not yet reached a temperature-independent rubbery plateau at 130 °C, most likely due to a broadened glass transition caused by oxidized surface layers, indicating that the calculated values in Table S1 overestimate the apparent crosslink density. However, comparing the experimentally determined values of Table S1 with the theoretically derived values (Section S5, cf. Table S2), which assume perfect stoichiometry, full conversion, and absence of network defects, reveals a clear discrepancy. This discrepancy underscores the importance of correcting for non-Gaussian chain statistics as outlined in the work of *Charlesworth* [86], when the density of elastically effective chains exceeds ~1.5 mol/kg (4.6 - 4.9 mol/kg in our case).

Overall, thermo-oxidative degradation manifests in counterintuitive effects expressed in: (i) increased rigidity and stiffness due to network densification and "internal antiplasticization", and (ii) decreased T_g due a crosslinking density decrease.

3.3. Effect of thermo-oxidative degradation on stress relaxation behavior

Tensile stress relaxation is conducted in a temperature range of 140 – 200 °C. Certainly, during testing, an effect of thermo-oxidative degradation is expected, but maximum residual times of 600 s at 200 °C keep the thermo-oxidative degradation induced during testing below 0.1 % (cf. Fig. 1d). We choose the Kohlrausch−Williams−Watts (KWW) stretched exponential decay [87] extended with a weight factor υ accounting for nonexchangeable fractions [88] to fit the tensile stress relaxation response for the different degradation states separately (Figure S10):

$$\frac{E(t)}{E_0} = (1-\upsilon)\cdot exp\left[-\left(\frac{t}{\tau^*}\right)^{\beta}\right] + \upsilon, \tag{7}$$

where τ^* represents the relaxation time, β the stretching exponent and $E(t)$ the decay in relaxation modulus at time t related to its initial value E_0. The β values ($0 < \beta \leq 1$) describe the width of the relaxation time distribution, with lower β values associated with greater width and more heterogeneous segmental dynamics [89]. In the case $\beta = 1$, a classical Debye relaxation process would take place. The parameters β and τ^* are fitted for each temperature and subsequently the average relaxation times are calculated as follows [90]:

$$\tau = \frac{\tau^* \Gamma\left(\frac{1}{\beta}\right)}{\beta}, \tag{8}$$

where Γ is the gamma function. The activation energies E_a of flow is calculated assuming an Arrhenius-like behavior of the average relaxation time $\langle\tau\rangle = \tau_0 \exp\left(\frac{E_a}{RT}\right)$, with E_a being calculated to 103 kJ/mol for the pristine state, which is in the range of disulfide vitrimers reported in literature [8,9,56,91]. Even across the investigated broad temperature range and different degradation states, an excellent Arrhenius-type temperature dependence of the relaxation times was obtained with R^2 located above 0.996 (Fig. 5d). The stretching coefficient β values (Fig. 5c) range from 0.58 to 0. 87 and depend on temperature, suggesting a gradual increase in relaxation homogeneity with increasing temperature. At elevated temperatures, the disulfide bonds situated within flexible chain segments are less influenced by segmental motion and can exchange more freely, resulting in a more singular relaxation process [92]. At lower temperatures, the effects of the glass transition become noticeable, partly constraining segmental motion and leading to a less singular relaxation process. Besides that, the thermo-oxidative degradation decreases the stretching coefficient β (β declining from ~ 0.87 to ~ 0.82 at 200 °C), suggesting a gradual increase of relaxation heterogeneity caused by the oxidized surface layer and selective breakage of disulfide crosslinks.

Tensile stress-relaxation trials of the degraded specimens (Fig. 5a) quantify the kinetics of disulfide-bond exchange for different degradation states. Fig. 5a shows the normalized stress relaxation data at 160 °C, and Fig. 5b shows $\langle\tau\rangle$ for different degradation states and temperatures. We observe a gradual decrease of the average relaxation time $\langle\tau\rangle$ by a factor of up to ~ 11 at 140 °C (Fig. 5b), showcasing the effect of increased mobility of remaining S-S bonds due to reduced network density ν_e (cf. Table S1). Besides, Thiol/thiyl species are better nucleophiles and may attack neighboring S-S bonds, therefore supporting the associative exchange. Even if the S-O formation causes a more dense network, the effect on chain scissions remains predominant and accelerates the relaxation.

These superimposed effects appear to be very effective in reducing relaxation times. Indeed, reduced relaxation times are desirable; however, they are accompanied by increased residual stresses at ~300 s (cf. Fig. 5a) and a notable linear increase in nonexchangeable network fractions (Fig. 6), indicating that the network loses its ability to relax fully. Based on this observation, it may be suggested that continuous thermo-oxidative degradation transforms dynamic S-S bonds into less dynamic species (e.g., oxidized sulfur species), thereby preventing complete stress relaxation within the network. The linear approximation remains limited to degradation values above 1 %, as values below that threshold produce artificially higher υ values (while still preserving the trend of increasing υ with degradation) because the system does not reach equilibrium stress state. Even for low degradation, the fitted υ parameters are sufficiently constrained by the data, as evidenced by small error bars (standard error of the fitted non-relaxing fraction parameter υ), likely due to the overall shape of the relaxation curves. However, it is important to note that although the least-squares fit may still yield small formal standard errors of υ (cf. Fig. 6), these values could underestimate the true uncertainty when the relaxation is not fully completed, as multiple parameter permutations can equally well describe the data set, yet not reflected in the formal standard error. Fig. 6 not only shows that continued degradation consistently increases the nonexchangeable network fraction, but also indicates that υ values decrease with increasing temperature because the equilibrium stress is not reached within the prescribed time scales. Notably, even for the

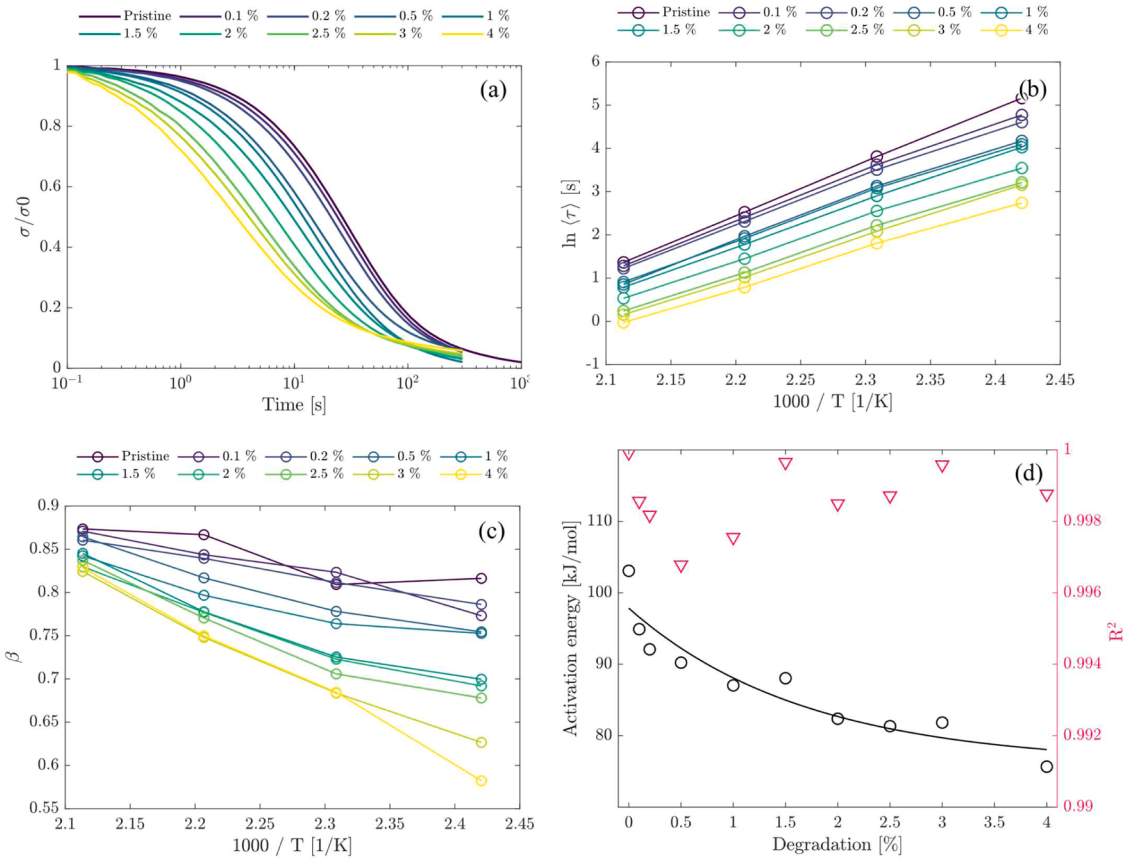

Fig. 5. Normalized stress relaxation of different degradation states at 160 °C (a). Degradation-dependence of average relaxation times $\langle\tau\rangle$ (b) and stretching exponent β (c). Activation energy depending on the degradation (d).

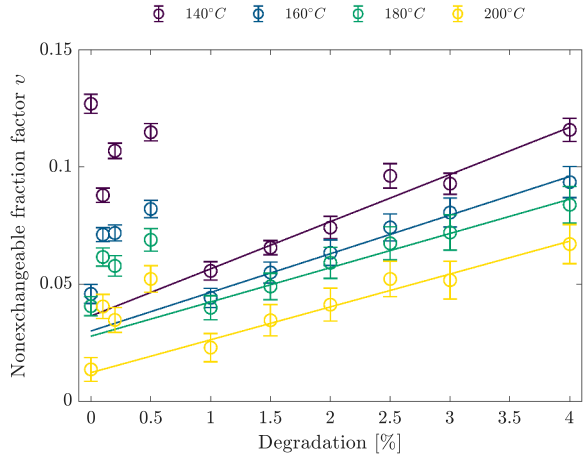

Fig. 6. Degradation-dependence of the nonexchangeable fraction factor υ for different temperatures.

pristine sample, relaxed at the highest temperature, final υ values of 0.01 are reached. As noted above, with the final force values ranging from 10–100 mN, we are operating at the low-force limits of the DMTA (~ 10 mN [85]). Therefore, caution should be exercised when interpreting the final force values, especially during the high-temperature relaxation steps.

Thus, as degradation increases, we observe a reduction in dynamic cross-links (as evidenced by reduced crosslinking density, cf. Table S1) and an inhibition of complete network relaxation (increased υ values after high levels of degradation, cf. Fig. 6), which are hypothesized to be associated with the transformation of dynamic S-S bonds into non-dynamic moieties. Besides, as might be expected given the reduced relaxation times, the activation energy for the dynamic bond exchange decreases (cf. Fig. 5d). While the presented results provide clear evidence of more rapid stress relaxation with increasing degradation, it remains challenging to deconvolute the underlying contributions of network connectivity changes (i) and 'true' chemical acceleration of S-S exchange (ii) (e.g., Thiol/thiyl species with enhanced nucleophilicity catalyzing the exchange of neighboring dynamic S-S bonds).

3.4. Evaluating the effect of thermo-oxidative aging for processing and testing protocols

It has been shown that thermo-oxidative aging influences the dynamic bond exchange kinetics and may reduce the time required for healing and malleability. Accordingly, the following section examines the implications for practical processing applications and testing protocols. First, the emergence of macroscopic flow, which is fundamental to all processes that exploit the malleability of vitrimers, is discussed. Second, the influence of thermo-oxidative aging on the outcome of stress relaxation experiments conducted over a wide temperature range, representative of typical testing conditions for disulfide vitrimers, is examined.

3.4.1. Initiation of macroscopic flow

The malleability of dynamic polymer networks and vitrimers has been of utmost interest in recent years, especially with regard to the question if the onset (or offset, depending on heating or cooling, respectively) of macroscopic flow can be considered as a type of transition phenomenon (in the sense of a glass or even a phase transition) or if it has purely dynamic origins. Not getting into the this discussion the

reader might be referred to [58,93–95]. Thermomechanical analyses has shown to be a suitable tool to at least qualitatively assess and compare the flowability of a given set of samples under a given set of boundary conditions (e.g., force, temperature rate). *Hubbard et al.* tested the thermally induced length change behavior of a model vitrimer via heating-controlled thermomechanical analysis. They found that sample lengths initially increased constantly with increasing temperature, predominantly driven by thermal expansion. Curiously, upon further heating, the sample lengths reached a peak value and decreased again. The authors assigned this behavior to a seemingly characteristic transition temperature T_v, above which dynamic covalent bond exchange-induced macroscopic flow compensated the simultaneously occurring thermal expansion [59]. Hence, it must be acknowledged that the material had begun to flow before reaching the peak value of the sample length changes. This renders the definition of such a transition temperature T_v *ad absurdum*, and T_v should, in this case, rather be considered as an operational processing parameter. Nevertheless, to evaluate and compare the flow-dominated behavior of a given vitrimer system, similar experiments were performed in this work (cf. Fig. 7). Beyond, e.g., the effect of temperature rate, applying a constant-force criterion to materials with differing stiffnesses is problematic because it violates the isostrain condition. Consequently, variations in the apparent flow initiation temperature (we have deliberately chosen not to use the term 'transition temperature') may reflect not only structural changes (i.e., changes in bond exchange rate and thus flow) but also additional contributions arising from differences in apparent strains. Therefore, selected measurements are also conducted under isostrain conditions (cf. Figure S12a). Note that we still cannot strictly guarantee isostrain conditions, as the modulus varies consistently with temperature, especially in the degraded samples with a broader transition region. Fig. 7b and Figure S12a suggest that the applied force has only a minor influence on the measured T_v. This is consistent with the observations in [58,59]. Therefore, we conclude that the major driving force behind the shift in the apparent flow initiation is actually morphological changes (carbonyl surface layer, crosslinking density) within the materials (considering the aforementioned boundary conditions). The circles in Fig. 7a identify the maximum values, indicating the temperature at which the vitrimer-inherent macroscopic flow compensates and overcomes thermal expansion.

Fig. 7a outlines that with increased degradation, the apparent flow initiation temperature shifts to lower values, implying that the shape reconfigurability of vitrimer exposed to thermo-oxidative aging may already be accessed at lower temperature regimes. In other words, the previously outlined faster bond exchanges and lower activation energies directly manifest as shifts in the initiation of macroscopic flow dominance. Still, oxidation itself may influence the physical properties, such as thermal conductivity. In particular, the formation of carbonyls has been reported to increase thermal conductivity [96]. Consequently, especially at high heating rates, a potential increase in thermal conductivity could lead to a premature temperature rise in the oxidized samples, thereby triggering earlier flow. Therefore, the observed premature macroscopic flow likely arises from structural changes within the material (i.e., accelerated bond exchange), while secondary effects, such as changes in thermal and mechanical boundaries, may also contribute.

From a practical perspective, this implies that shorter holding times are sufficient for healing and shape reconfiguration, and that the (re) processing regime may be shifted to lower temperatures, not considering altered healing capabilities due to the differently degraded states. Therefore, it remains to be clarified to what extent this advantageous result can be maintained across multiple reprocessing cycles, calling for more in-depth characterisation.

To provide another perspective on the thermally induced shape change behavior of the differently degraded disulfide vitrimers, Fig. 8 shows the normalized sample lengths obtained from a TMA cooling experiment.

To avoid initial metastability in the system, the material was heated to 190 °C and cooled to 0 °C at 1K/min. A tracking force of 0.1 N was applied throughout the measurement. The continuous slope changes indicate the system's shape change behavior that ultimately stops only

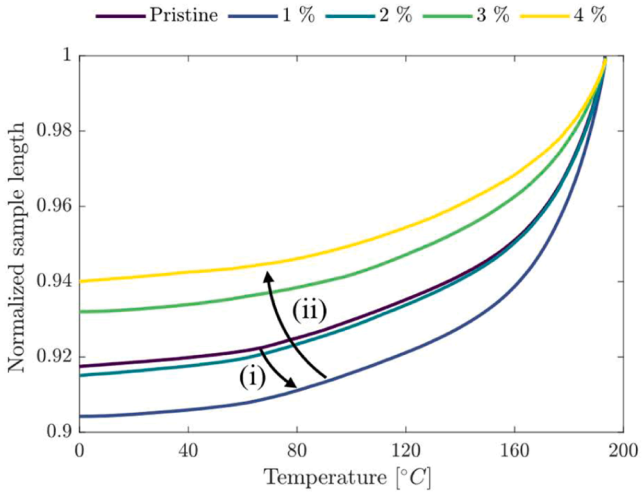

Fig. 8. Normalized sample length during cooling using a tracking force of 0.1 N.

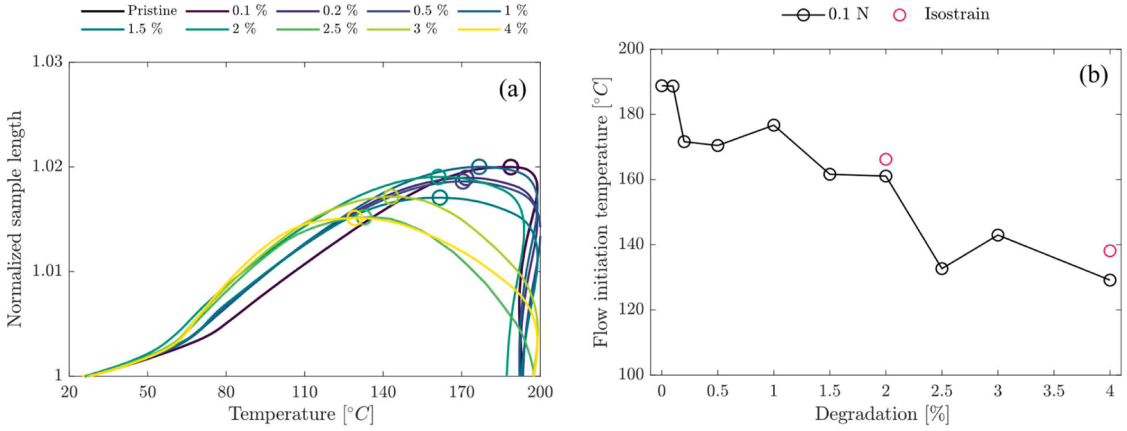

Fig. 7. Normalized sample length change during the heated thermomechanical analysis. Maximum values indicate initiation of macroscopic flow (a). Flow initiation temperature as a function of degradation under constant force and isostrain conditions (b).

at the thermal glass transition [58]. However, the most essential aspect of the degradation effect is that the shape change behavior is indeed accelerated at first (i). The normalized sample length change initially increases from the pristine sample to the 1 % degradation sample, supporting the idea of permanently cleaved S-S bonds. Though, in contrast to the fast-heating measurements (Fig. 7), isostrain measurements during cooling (Figure S12b) reveal a significant effect of the applied force on the sample length change, especially above 130 °C. Under these conditions, the contribution of strain can no longer be neglected. Therefore, any conclusions can address only the combined effects of structural changes within the material and strain dependence. This superposition state corresponds to the typical boundary conditions of a forming process in which compression is carried out under a constant load, thereby providing implications for practical processing. In detail, upon further degradation, from 2 % to 3 % to 4 %, the total shape-changing capabilities of the materials diminish (ii), re-emphasizing the hypothesized gradual formation of permanent bonds (justified by increased non-exchangeable fractions, cf. Fig. 6). Even though the data shown in Fig. 7 were obtained under non-stable heating conditions with very high heating rates (20 K/min), the data are surprisingly in agreement with the TMA-dataset obtained from the cooling experiments (Fig. 8): at increased degradation states above 2.5 %, the flowability of the vitrimer systems remains close to constant.

3.4.2. Stress relaxation experiments under confined conditions

Besides, the presence of thermo-oxidative aging raises the question of how it influences stress relaxation experiments and at what temperature these effects become measurable and significant. Therefore, the stress relaxation behavior of the pristine vitrimer system at temperatures ranging from 140 to 210 °C was repeatedly tested (4 times). Each temperature step includes an initial 5 min isothermal dwell, followed by instantaneous application of 1 % strain and recording the relaxation for 15 min, thereby exposing the material to 20 min at the designated temperature. The calculated normalized average relaxation times $\langle\tau\rangle$ and stretching exponents β for the repeated testing are provided in Fig. 9.

As can be seen, isothermal dwelling at the lower temperatures causes a continuous increase of $\langle\tau\rangle$ and homogenize the relaxation time distribution, indicating a more homogeneous network structure attributed to residual crosslinking. Above 190 °C, these trends reverse and $\langle\tau\rangle$ decrease while β decreases, meaning that selective cleavage of disulfide bonds becomes apparent. As network density decreases, more rapid exchange reactions are facilitated. Translating the applied time-temperature profiles into the degradation domain using the derived kinetic degradation model yields a threshold of 2 %, above which a noticeable effect on the relaxation times is observed (cf. Fig. 10).

Subsequent ramped heating (cf. Figure S15) reveals a decrease in primary T_g and a secondary peak formation as previously discussed. As it is common practice to conduct stress relaxation on a single specimen by sequentially sweeping through different temperatures, accumulated degradation may impair the apparent relaxation time and the derived activation energy. To quantify this circumstance, Figure S16 and Table S3 show the determination of bond exchange activation energy for three different cases: a pristine sample is used for each temperature step (i), the temperature steps are imposed consecutively on a sample with dwell times of 20 min (ii) and 60 min (iii), respectively. The apparent relaxation times are linearly interpolated and extrapolated depending on the current state of degradation from Fig. 10. Deriving the activation energies for cases (i)-(iii) reveals that the effect of degradation may also be accompanied by up to 15 % increased activation energies. Thus, thermo-oxidative aging at elevated temperatures accelerates relaxation behaviour and, consequently, can lead to an overestimation of the derived activation energies. For this reason, the dwell times under isothermal conditions should be carefully selected, e.g., by terminating the measurement after the normalized relaxation modulus has dropped below 1/e, thereby minimizing the overall dwell time.

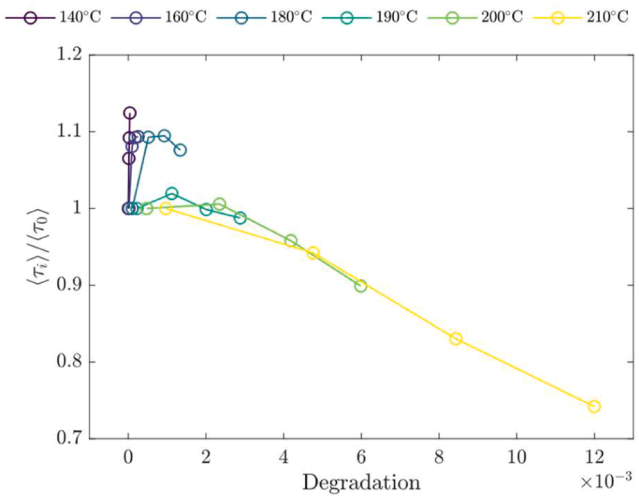

Fig. 10. Normalised average relaxation times $\langle\tau_i\rangle/\langle\tau_0\rangle$ as a function of apparent degradation calculated according to Eq. (6).

4. Conclusion

In conclusion, by selectively tailoring the thermo-oxidative degradation of specimens, while simultaneously using kinetic modeling, the isolated effect of degradation on the viscoelastic response of the

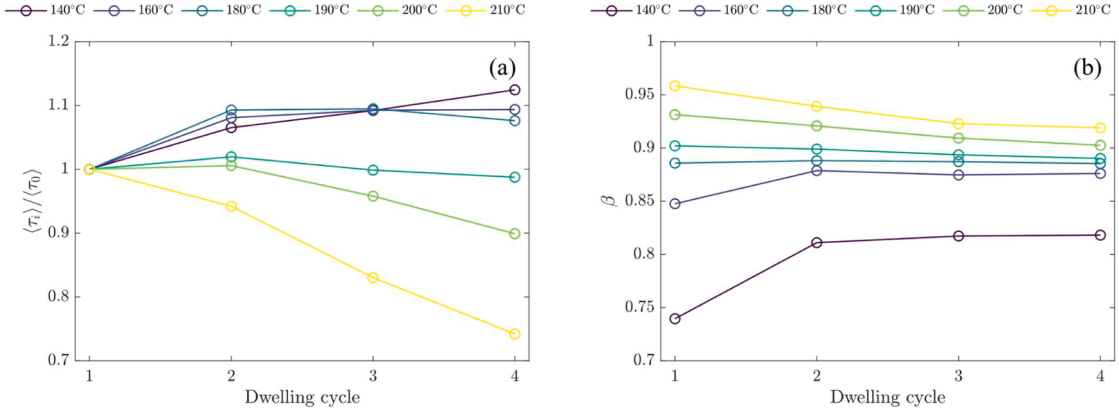

Fig. 9. Effect of different repeated isothermal dwellings on the predicted normalised average relaxation times $\langle\tau_i\rangle/\langle\tau_0\rangle$ (a) Stretching exponent β (b). Corresponding relaxation times for (a) are provided in Figure S14.

disulfide-based epoxy vitrimer is examined. Increasing degradation is accompanied by a continuous decrease in the primary T_g, while the increasing peak width of the transition and FTIR analysis suggests the formation of carbonyl at the surface, proposing a "skin-core" structure within the cross-section. Although multiple observations (secondary tan δ peak, carbonyl growth, and increased nonexchangeable network fraction) are consistent with the formation of a 'skin-core' structure, the evidence remains indirect and calls for a more detailed, spatially resolved analysis to determine its thickness and compositional heterogeneity conclusively.

The stress-relaxation times, which are directly coupled to the bond-exchange kinetics, decrease substantially with increasing degradation, leading to lower activation energies for the dynamic bond exchanges. Though based on the present results, it remains challenging to deconvolute the relative contributions of network connectivity changes (i), as evidenced by reduced crosslinking density with degradation, and intrinsic changes in the exchange kinetics (ii).

This favourable faster relaxation directly manifests as shifts in the initiation of macroscopic flow under isoforce conditions, serving as a processing indicator for shifting the (re)processing regime to lower temperatures. The observed premature macroscopic flow likely arises from structural changes within the material (i.e., accelerated bond exchange), while secondary effects, such as changes in thermal and mechanical boundaries, also contribute. Therefore, we cannot conclude a universal shift of the vitrimer transition T_v but solely report an overall advanced malleability in the degraded states.

However, in the long run, cleavage and oxidation of the dynamic S-S crosslinks may become predominant, adversely compromising the dynamic properties of these systems, as evidenced by incomplete relaxation and increased nonexchangeable network fraction. Therefore, the balance between network degradation via dynamic bond cleavage (changes in network connectivity) and oxidative deactivation of these bonds appears to govern the residual fluidity imparted by the remaining dynamic bonds. Nevertheless, further investigation into how the temperature dependence of the storage modulus influences the predominant stress state in bulk samples would strengthen the reliability of this conclusion. Decoupling mechanical loading, plasticity, and the apparent flow of the material within a multi-physics simulation may help resolve that uncertainty and link the relaxation time to apparent bond-exchange capabilities quantified by macroscopic flow.

These insights into the distinct effects of thermal degradation and thermo-oxidative aging provide a robust foundation for evaluating long-term performance following high-temperature exposure in oxygen-containing environments and have important implications for the design of appropriate testing protocols and (re)processing strategies for disulfide-based epoxy vitrimers.

Data availability

Data for this article, including all diagram data are available at 4TU. Research at https://doi.org/10.4121/c492c748-150d-411f-8cd8-3d29487b257f.

CRediT authorship contribution statement

Niklas Lorenz: Writing – original draft, Visualization, Validation, Methodology, Investigation, Formal analysis, Data curation, Conceptualization. **Andreas Klingler:** Writing – review & editing, Validation, Methodology, Investigation, Formal analysis, Conceptualization. **William E. Dyer:** Writing – review & editing. **Santiago J. Garcia:** Writing – review & editing, Formal analysis. **Baris Kumru:** Writing – review & editing, Funding acquisition.

Declaration of competing interest

The authors declare that they have no known competing financial interests or personal relationships that could have appeared to influence the work reported in this paper.

Niklas Lorenz reports financial support was provided by Delft University of Technology. Niklas Lorenz reports a relationship with Delft University of Technology that includes: employment. If there are other authors, they declare that they have no known competing financial interests or personal relationships that could have appeared to influence the work reported in this paper.

Acknowledgments

This project is made possible partly by a contribution from the National Growth Fund program NXTGEN HIGHTECH 01 (NGFNH2201). The authors acknowledge continuous support from the ASM department and technical staff. Parts of the research were carried out within the COMET-Module project "Repairtecture" (project no.: 904927) at the Polymer Competence Center Leoben GmbH (PCCL, Austria) within the framework of the COMET program of the Federal Ministry for Climate Action, Environment, Energy, Mobility, Innovation, and Technology and the Federal Ministry of Labour and Economy. Funding was provided by the Austrian Government and the State Governments of Styria and Upper Austria.

Supplementary materials

Supplementary material associated with this article can be found, in the online version, at doi:10.1016/j.polymdegradstab.2026.112140.

References

[1] S. Maes, N. Badi, J.M. Winne, F.E. Du Prez, Taking dynamic covalent chemistry out of the lab and into reprocessable industrial thermosets, Nat. Rev. Chem. 9 (2025) 144–158, https://doi.org/10.1038/s41570-025-00686-7.
[2] Y. Yang, Y. Xu, Y. Ji, Y. Wei, Functional epoxy vitrimers and composites, Prog. Mater. Sci. 120 (2021) 100710, https://doi.org/10.1016/j.pmatsci.2020.100710.
[3] H. Memon, Y. Wei, C. Zhu, Recyclable and reformable epoxy resins based on dynamic covalent bonds – Present, past, and future, Polym. Test. 105 (2022) 107420, https://doi.org/10.1016/j.polymertesting.2021.107420.
[4] J. Zheng, Z.M. Png, S.H. Ng, G.X. Tham, E. Ye, S.S. Goh, X.J. Loh, Z. Li, Vitrimers: current research trends and their emerging applications, Mater. Today 51 (2021) 586–625, https://doi.org/10.1016/j.mattod.2021.07.003.
[5] M. AbdolahZadeh, A.C.C. Esteves, S. van der Zwaag, S.J. Garcia, Healable dual organic–inorganic crosslinked sol–gel based polymers: crosslinking density and tetrasulfide content effect, J. Polym. Sci. A: Polym. Chem. 52 (2014) 1953–1961, https://doi.org/10.1002/pola.27200.
[6] D. Montarnal, M. Capelot, F. Tournilhac, L. Leibler, Silica-like malleable materials from permanent organic networks, Science 334 (2011) 965–968, https://doi.org/10.1126/science.1212648.
[7] B. Lewis, J.M. Dennis, C. Park, K.R. Shull, Glassy dynamics of epoxy-amine thermosets containing dynamic, aromatic disulfides, Macromolecules 57 (2024) 7112–7122, https://doi.org/10.1021/acs.macromol.4c01012.
[8] I. Azcune, E. Elorza, A. Ruiz De Luzuriaga, A. Huegun, A. Rekondo, H.-J. Grande, Analysis of the effect of network structure and disulfide concentration on vitrimer properties, Polym. (Basel) 15 (2023) 4123, https://doi.org/10.3390/polym15204123.
[9] A. Ruiz de Luzuriaga, G. Solera, I. Azcarate-Ascasua, V. Boucher, H.-J. Grande, A. Rekondo, Chemical control of the aromatic disulfide exchange kinetics for tailor-made epoxy vitrimers, Polym. (Guildf) 239 (2022) 124457, https://doi.org/10.1016/j.polymer.2021.124457.
[10] N. Lorenz, W.E. Dyer, B. Kumru, High-performance vitrimer entailing renewable plasticizer engineered for processability and reactivity toward composite applications, ACS. Appl. Polym. Mater. 7 (2025) 1934–1946, https://doi.org/10.1021/acsapm.4c03731.
[11] S. Zhao, M.M. Abu-Omar, Recyclable and malleable epoxy thermoset bearing aromatic imine bonds, Macromolecules. 51 (2018) 9816–9824, https://doi.org/10.1021/acs.macromol.8b01976.
[12] B. Li, G. Zhu, Y. Hao, T. Ren, Effect of cross-link density on the performance of polyimine/epoxy vitrimers, Smart. Mater. Struct. 33 (2024) 025014, https://doi.org/10.1088/1361-665X/ad1c54.
[13] N. Lorenz, W.E. Dyer, B. Kumru, Thermo-rheological and kinetic characterization and modeling of an epoxy vitrimer based on polyimine exchange, Soft. Matter 20 (2024) 6289–6301, https://doi.org/10.1039/D4SM00724G.
[14] V. Amfilochiou, T. Debsharma, I. De Baere, L. Daelemans, F. Du Prez, W. Van Paepegem, Thermomechanical characterisation of reprocessable, siloxane-based, glass-fibre-reinforced vitrimers, Compos. B: Eng. 276 (2024) 111354, https://doi.org/10.1016/j.compositesb.2024.111354.

[15] T. Debsharma, V. Amfilochiou, A.A. Wróblewska, I. De Baere, W. Van Paepegem, F. E. Du Prez, Fast dynamic siloxane exchange mechanism for reshapable vitrimer composites, J. Am. Chem. Soc. 144 (2022) 12280–12289, https://doi.org/10.1021/jacs.2c03518.

[16] W. Denissen, G. Rivero, R. Nicolaÿ, L. Leibler, J.M. Winne, F.E. Du Prez, Vinylogous urethane vitrimers, Adv Funct Mater. 25 (2015) 2451–2457, https://doi.org/10.1002/adfm.201404553.

[17] W. Alabiso, S. Schlögl, The impact of vitrimers on the industry of the future: chemistry, properties and sustainable forward-looking applications, Polymers. (Basel) 12 (2020) 1660, https://doi.org/10.3390/polym12081660.

[18] B. Krishnakumar, R.V.S.P. Sanka, W.H. Binder, V. Parthasarthy, S. Rana, N. Karak, Vitrimers: associative dynamic covalent adaptive networks in thermoset polymers, Chem. Eng. J. 385 (2020) 123820, https://doi.org/10.1016/j.cej.2019.123820.

[19] V. Schenk, K. Labastie, M. Destarac, P. Olivier, M. Guerre, Vitrimer composites: current status and future challenges, Mater. Adv. 3 (2022) 8012–8029, https://doi.org/10.1039/D2MA00654E.

[20] N. Lorenz, T. Zawadzki, L. Keller, J. Fuchs, K. Fischer, C. Hopmann, Characterization and modeling of an epoxy vitrimer based on disulfide exchange for wet filament winding applications, Polym. Eng. Sci. 64 (2024) 3682–3702, https://doi.org/10.1002/pen.26805.

[21] W.E. Dyer, B. Kumru, Polymers as aerospace structural components: how to reach sustainability? Macromol. Chem. Phys. 224 (2023) 2300186 https://doi.org/10.1002/macp.202300186.

[22] V. Schenk, R. D'Elia, P. Olivier, K. Labastie, M. Destarac, M. Guerre, Exploring the limits of high-T(g) epoxy vitrimers produced through resin-transfer molding, ACS. Appl. Mater. Interfaces. 15 (2023) 46357–46367, https://doi.org/10.1021/acsami.3c10007.

[23] A.M. Hubbard, Y. Ren, A. Sarvestani, D. Konkolewicz, C.R. Picu, A.K. Roy, V. Varshney, D. Nepal, Recyclability of vitrimer materials: impact of catalyst and processing conditions, ACS. Omega 7 (2022) 29125–29134, https://doi.org/10.1021/acsomega.2c02677.

[24] V. Boulic, D.A. Boina, M. Staropoli, S. Westermann, P. Verge, D.F. Schmidt, F. Addiego, Insights into the mechanism of vitrimer reconsolidation via X-ray tomography, Polym. Test. 152 (2025) 109006, https://doi.org/10.1016/j.polymertesting.2025.109006.

[25] H. Zhang, J. Cui, G. Hu, B. Zhang, Recycling strategies for vitrimers, Int. J. Smart. Nano Mater. 13 (2022) 367–390, https://doi.org/10.1080/19475411.2022.2087785.

[26] R. Hayder, S. Kedziora, Cyclic healing of delamination in amine-epoxy vitrimer carbon fiber composites, Results. Eng. 28 (2025) 107405, https://doi.org/10.1016/j.rineng.2025.107405.

[27] H. Perrin, R. Vaudemont, D. Del Frari, P. Verge, L. Puchot, M. Bodaghi, On the cyclic delamination-healing capacity of vitrimer-based composite laminates, Compos. A: Appl. Sci. Manuf. 177 (2024) 107899, https://doi.org/10.1016/j.compositesa.2023.107899.

[28] P.R. Barnett, J.A. Brackenridge, A.A. Advincula, L.A. Taussig, D. Nepal, Reformable and sustainable thermosetting carbon fiber composites from epoxy vitrimer, Compos. B: Eng. 274 (2024) 111270, https://doi.org/10.1016/j.compositesb.2024.111270.

[29] I.M. Hodge, Physical aging in polymer glasses, Science (1979) 267 (1995) 1945–1947, https://doi.org/10.1126/science.267.5206.1945.

[30] G.M. Odegard, A. Bandyopadhyay, Physical aging of epoxy polymers and their composites, J. Polym. Sci. B: Polym. Phys. 49 (2011) 1695–1716, https://doi.org/10.1002/polb.22384.

[31] I. Kada, D. Trinh, S. Touzain, S. Mallarino, Quantification of physical aging using two MDSC methods and its effect on initial properties of epoxy films, J. Non. Cryst. Solids. 649 (2025) 123335, https://doi.org/10.1016/j.jnoncrysol.2024.123335.

[32] S.L. Maddox, J.K. Gillham, Isothermal physical aging of a fully cured epoxy—Amine thermosetting system, J. Appl. Polym. Sci. 64 (1997) 55–67, https://doi.org/10.1002/(SICI)1097-4628(19970404)64:1%253C55::AID-APP5%253E3.0.CO;2-Q.

[33] C. Bockenheimer, D. Fata, W. Possart, New aspects of aging in epoxy networks. I. Thermal aging, J. Appl. Polym. Sci. 91 (2004) 361–368, https://doi.org/10.1002/app.13092.

[34] Y. Pei, K. Wang, M. Zhan, W. Xu, X. Ding, Thermal-oxidative aging of DGEBA/EPN/LMPA epoxy system: chemical structure and thermal–mechanical properties, Polym. Degrad. Stab. 96 (2011) 1179–1186, https://doi.org/10.1016/j.polymdegradstab.2011.04.019.

[35] B. Jewell, T. Sain, From network degradation to mechanical brittleness: the aging response of epoxy vitrimers, Polym. Degrad. Stab. 242 (2025) 111654, https://doi.org/10.1016/j.polymdegradstab.2025.111654.

[36] E. Ernault, J. Dirrenberger, E. Richaud, B. Fayolle, Prediction of stress induced by heterogeneous oxidation: case of epoxy/amine networks, Polym. Degrad. Stab. 162 (2019) 112–121, https://doi.org/10.1016/j.polymdegradstab.2019.02.019.

[37] N. Rasoldier, X. Colin, J. Verdu, M. Bocquet, L. Olivier, L. Chocinski-Arnault, M. C. Lafarie-Frenot, Model systems for thermo-oxidised epoxy composite matrices, Compos. A: Appl. Sci. Manuf. 39 (2008) 1522–1529, https://doi.org/10.1016/j.compositesa.2008.05.016.

[38] J.-S. Chen, C.K. Ober, M.D. Poliks, Y. Zhang, U. Wiesner, C. Cohen, Controlled degradation of epoxy networks: analysis of crosslink density and glass transition temperature changes in thermally reworkable thermosets, Polym. (Guildf) 45 (2004) 1939–1950, https://doi.org/10.1016/j.polymer.2004.01.011.

[39] B. Jewell, P.P. Abadi, T. Sain, Experimental characterization and constitutive modeling of bulk epoxy under thermo-oxidative aging, Polym. Degrad. Stab. 234 (2025) 111215, https://doi.org/10.1016/j.polymdegradstab.2025.111215.

[40] M. Pecora, Y. Pannier, M.-C. Lafarie-Frenot, M. Gigliotti, C. Guigon, Effect of thermo-oxidation on the failure properties of an epoxy resin, Polym. Test. 52 (2016) 209–217, https://doi.org/10.1016/j.polymertesting.2016.04.008.

[41] L. Olivier, N.Q. Ho, J.C. Grandidier, M.C. Lafarie-Frenot, Characterization by ultra-micro indentation of an oxidized epoxy polymer: correlation with the predictions of a kinetic model of oxidation, Polym. Degrad. Stab. 93 (2008) 489–497, https://doi.org/10.1016/j.polymdegradstab.2007.11.012.

[42] Z. Fang, X. Gao, Y. Sun, M. Zhang, D. Wen, Y. Gao, S. Cheng, T. Liu, Evolution in properties of carbon fiber reinforced vitrimer composites after thermo-oxidative aging, Compos. Commun. 46 (2024) 101846, https://doi.org/10.1016/j.coco.2024.101846.

[43] Z. Wu, Z. Zhang, Q. Zhu, W. Guo, J. Li, Q. Zhang, C. Gao, G. Wang, A critical examination of transesterification-based vitrimer with a focus on hygrothermal aging stability, J. Appl. Polym. Sci. 143 (2026) e58071, https://doi.org/10.1002/app.58071.

[44] D. Sanchez-Rodriguez, S. Zaidi, Y. Jahani, A. Ruiz De Luzuriaga, A. Rekondo, P. Maimi, J. Farjas, J. Costa, Processability and reprocessability maps for vitrimers considering thermal degradation and thermal gradients, Polym. Degrad. Stab. 217 (2023) 110543, https://doi.org/10.1016/j.polymdegradstab.2023.110543.

[45] D. Sanchez-Rodriguez, S. Zaidi, L. Carreras, A. Ruiz de Luzuriaga, A. Rekondo, J. Costa, J. Farjas, Time-temperature-transformation diagrams from isoconversional kinetic analyses applied to the processing and reprocessing of vitrimers, Thermochim. Acta 736 (2024) 179744, https://doi.org/10.1016/j.tca.2024.179744.

[46] S. Yang, S. Zhang, F. Luo, H. Li, F. Xiao, Curing and thermal degradation behavior of epoxy-based vitrimers, J Appl. Polym. Sci 141 (2024) e55057, https://doi.org/10.1002/app.55057.

[47] P. Fanlo, A. Ruiz De Luzuriaga, G. Albizu, M. Ximenis, A. Rekondo, H.J. Grande, H. Sardon, Unraveling the thermal stability of aromatic disulfide epoxy vitrimers: a comprehensive study using principal component analysis (PCA), RSC Appl. Polym. 2 (2024) 826–837, https://doi.org/10.1039/D4LP00156G.

[48] H. Sharma, R. Patel, S. Rana, Epoxy vitrimers: effect of thermal cycling on stress relaxation and self-healing properties, ChemistrySelect. 10 (2025) e01491, https://doi.org/10.1002/slct.202501491.

[49] A.G. Vandeputte, M.-F. Reyniers, G.B. Marin, Theoretical study of the thermal decomposition of dimethyl disulfide, J. Phys. Chem. A 114 (2010) 10531–10549, https://doi.org/10.1021/jp103357z.

[50] J. Liang, J.M. Fernández, Kinetic measurements on single-molecule disulfide bond cleavage, J. Am. Chem. Soc. 133 (2011) 3528–3534, https://doi.org/10.1021/ja109684q.

[51] Y. Xia, F. Zhou, W. Hao, S. Tang, Synthesis of degradable polyolefins bearing disulfide units via metathesis copolymerization, Polym. (Basel) 15 (2023) 3101, https://doi.org/10.3390/polym15143101.

[52] H. Hu, Q. Luan, J. Li, C. Lin, X. Ouyang, D.-Q. Wei, J. Wang, J. Zhu, High-molecular-weight and light-colored disulfide-bond-embedded polyesters: accelerated hydrolysis triggered by redox responsiveness, Biomacromolecules. 24 (2023) 5722–5736, https://doi.org/10.1021/acs.biomac.3c00691.

[53] L. Zhou, M. Chen, X. Zhao, Rapid degradation of disulfide-based thermosets through thiol-disulfide exchange reaction, Polym. (Guildf) 120 (2017) 1–8, https://doi.org/10.1016/j.polymer.2017.05.015.

[54] J. Wang, P. Sun, Z. Zheng, F. Wang, X. Wang, Glutathione-responsive biodegradable polyurethanes based on dithiodiundecanol, Polym. Degrad. Stab. 97 (2012) 2294–2300. https://doi.org/10.1016/j.polymdegradstab.2012.07.041.

[55] T. Ren, C. Wan, P. Song, D. Rodrigue, Y. Zhang, S. Wang, Thermo-oxidative degradation behavior of natural rubber vulcanized by different curing systems, Chem. Eng. Sci. 295 (2024) 120147, https://doi.org/10.1016/j.ces.2024.120147.

[56] N. Lorenz, W.E. Dyer, B. Kumru, Exploring the cure State dependence of relaxation and the vitrimer transition phenomena of a disulfide-based epoxy vitrimer, J. Polym. Sci. 63 (2025) 3739–3751, https://doi.org/10.1002/pol.20250463.

[57] P. Fanlo, O. Konuray, O. Ochoteco, M. Ximenis, A. Rekondo, H.Jürgen Grande, X. Fernández-Francos, H. Sardon, A.R. de Luzuriaga, Dynamic by design: unlocking full relaxation in disulfide epoxy networks, Polym. Chem. 16 (2025) 2701–2717, https://doi.org/10.1039/D5PY00124B.

[58] A. Klingler, D. Reisinger, S. Schlögl, B. Wetzel, U. Breuer, J.-K. Krüger, Vitrimer transition phenomena from the perspective of thermal volume expansion and shape (In)stability, Macromolecules. 57 (2024) 4246–4253, https://doi.org/10.1021/acs.macromol.4c00207.

[59] A.M. Hubbard, Y. Ren, A. Sarvestani, C.R. Picu, V. Varshney, D. Nepal, Thermomechanical analysis (TMA) of vitrimers, Polym. Test. 118 (2023), https://doi.org/10.1016/j.polymertesting.2022.107877.

[60] S. Kaiser, P. Novak, M. Giebler, M. Gschwandl, P. Novak, G. Pilz, M. Morak, S. Schlögl, The crucial role of external force in the estimation of the topology freezing transition temperature of vitrimers by elongational creep measurements, Polym. 204 (2020) 122804, https://doi.org/10.1016/j.polymer.2020.122804.

[61] A.M. Hubbard, Y. Ren, D. Konkolewicz, A. Sarvestani, C.R. Picu, G.S. Kedziora, A. Roy, V. Varshney, D. Nepal, Vitrimer transition temperature identification: coupling various thermomechanical methodologies, ACS. Appl. Polym. Mater. 3 (2021) 1756–1766, https://doi.org/10.1021/acsapm.0c01290.

[62] Y. Yang, S. Zhang, X. Zhang, L. Gao, Y. Wei, Y. Ji, Detecting topology freezing transition temperature of vitrimers by AIE luminogens, Nat. Commun. 10 (2019) 3165, https://doi.org/10.1038/s41467-019-11144-6.

[63] D. Sanchez-Rodriguez, S. Zaidi, Y. Jahani, A. Ruiz De Luzuriaga, A. Rekondo, P. Maimi, J. Farjas, J. Costa, Processability and reprocessability maps for vitrimers considering thermal degradation and thermal gradients, Polym. Degrad. Stab. 217 (2023) 110543, https://doi.org/10.1016/j.polymdegradstab.2023.110543.

[64] P. Das, P. Tiwari, Thermal degradation kinetics of plastics and model selection, Thermochim. Acta 654 (2017) 191–202, https://doi.org/10.1016/j.tca.2017.06.001.
[65] N. Sbirrazzuoli, Determination of pre-exponential factors and of the mathematical functions f(α) or G(α) that describe the reaction mechanism in a model-free way, Thermochim. Acta 564 (2013) 59–69, https://doi.org/10.1016/j.tca.2013.04.015.
[66] C.K. Tziamtzi, K. Chrissafis, Optimization of a commercial epoxy curing cycle via DSC data kinetics modelling and TTT plot construction, Polym. 230 (2021) 124091, https://doi.org/10.1016/j.polymer.2021.124091.
[67] S. Vyazovkin, Isoconversional kinetics of thermally stimulated processes, Springer Cham, 2015. https://doi.org/10.1007/978-3-319-14175-6, 978-3-319-14174-9.
[68] S. Vyazovkin, A.K. Burnham, J.M. Criado, L.A. Pérez-Maqueda, C. Popescu, N. Sbirrazzuoli, ICTAC Kinetics Committee recommendations for performing kinetic computations on thermal analysis data, Thermochim. Acta 520 (2011) 1–19, https://doi.org/10.1016/j.tca.2011.03.034.
[69] H.L. Friedman, Kinetics of thermal degradation of char-forming plastics from thermogravimetry. Application to a phenolic plastic, J. Polym. Sci. C: Polym. Symp. 6 (1964) 183–195, https://doi.org/10.1002/polc.5070060121.
[70] J. Farjas, P. Roura, Isoconversional analysis of solid-state transformations: a critical review. Part III. Isothermal and non isothermal predictions, J. Therm. Anal. Calorim. 109 (2012) 183–191, https://doi.org/10.1007/s10973-011-1642-2.
[71] J.A. Huidobro, I. Iglesias, B.F. Alfonso, A. Espina, C. Trobajo, J.R. Garcia, Reducing the effects of noise in the calculation of activation energy by the Friedman method, Chemom. Intell. Lab. Syst. 151 (2016) 146–152, https://doi.org/10.1016/j.chemolab.2015.12.012.
[72] J. Rieger, The glass transition temperature tg of polymers—Comparison of the values from differential thermal analysis (DTA, DSC) and dynamic mechanical measurements (torsion pendulum), Polym. Test. 20 (2001) 199–204, https://doi.org/10.1016/S0142-9418(00)00023-4.
[73] Z. Lei, W. Xing, J. Wu, G. Huang, X. Wang, L. Zhao, The proper glass transition temperature of amorphous polymers on dynamic mechanical spectra, J. Therm. Anal. Calorim. 116 (2014) 447–453, https://doi.org/10.1007/s10973-013-3526-0.
[74] A.R. Jagtap, A. More, Developments in reactive diluents: a review, Polym. Bull. 79 (2022) 5667–5708, https://doi.org/10.1007/s00289-021-03808-5.
[75] M. Khalina, M.H. Beheshty, A. Salimi, The effect of reactive diluent on mechanical properties and microstructure of epoxy resins, Polym. Bull. 76 (2019) 3905–3927, https://doi.org/10.1007/s00289-018-2577-6.
[76] L. Núñez-Regueira, M. Villanueva, I. Fraga-Rivas, Effect of a reactive diluent on the curing and dynamomechanical properties of an epoxy-diamine system, J. Therm. Anal. Calorim. 86 (2006) 463–468, https://doi.org/10.1007/s10973-005-7191-9.
[77] L. Audouin, V. Langlois, J. Verdu, J.C.M. De Bruijn, Role of oxygen diffusion in polymer ageing: kinetic and mechanical aspects, J. Mater. Sci. 29 (1994) 569–583, https://doi.org/10.1007/BF00445968.
[78] J. Delozanne, N. Desgardin, M. Coulaud, N. Cuvillier, E. Richaud, Failure of epoxies bonded assemblies: comparison of thermal and humid ageing, J. Adhes. 96 (2020) 945–968, https://doi.org/10.1080/00218464.2018.1547198.
[79] X. Colin, C. Marais, J. Verdu, A new method for predicting the thermal oxidation of thermoset matrices: application to an amine crosslinked epoxy, Polym. Test. 20 (2001) 795–803, https://doi.org/10.1016/S0142-9418(01)00021-6.
[80] J.P.M. Costa, X. Colin, Finite element modelling of the oxidation gradients of epoxy-diamine matrices below and above their glass transition temperature, Polym. Degrad. Stab. 234 (2025) 111194, https://doi.org/10.1016/j.polymdegradstab.2025.111194.
[81] R. Delannoy, V. Tognetti, E. Richaud, Experimental and theoretical insights on the thermal oxidation of epoxy-amine networks, Polym. Degrad. Stab. 206 (2022) 110188, https://doi.org/10.1016/j.polymdegradstab.2022.110188.
[82] J. Delozanne, N. Desgardin, N. Cuvillier, E. Richaud, Thermal oxidation of aromatic epoxy-diamine networks, Polym. Degrad. Stab. 166 (2019) 174–187, https://doi.org/10.1016/j.polymdegradstab.2019.05.030.
[83] B. Ellis, Chemistry and technology of epoxy resins, 1993.Springer Dordrecht; https://doi.org/10.1007/978-94-011-2932-9.
[84] R.A. Venditti, J.K. Gillham, Anomalous behavior of thermosetting systems after cure vs. chemical conversion: a normalized conversion–temperature–property diagram, J. Appl. Polym. Sci. 56 (1995) 1687–1705, https://doi.org/10.1002/app.1995.070561301.
[85] M. Müller-Pabel, J.A. Rodríguez Agudo, M. Gude, Measuring and understanding cure-dependent viscoelastic properties of epoxy resin: a review, Polym. Test. 114 (2022) 107701, https://doi.org/10.1016/j.polymertesting.2022.107701.
[86] J.M. Charlesworth, Effect of crosslink density on molecular relaxations in diepoxide-diamine network polymers. Part 2. The rubbery plateau region, Polym. Eng. Sci. 28 (1988) 230–236, https://doi.org/10.1002/pen.760280406.
[87] G. Williams, D.C. Watts, Non-symmetrical dielectric relaxation behaviour arising from a simple empirical decay function, Trans. Faraday Soc. 66 (1970) 80–85, https://doi.org/10.1039/TF9706600080.
[88] F. Meng, M.O. Saed, E.M. Terentjev, Elasticity and relaxation in full and partial vitrimer networks, Macromolecules. 52 (2019) 7423–7429, https://doi.org/10.1021/acs.macromol.9b01123.
[89] R.A. Riggleman, H.-N. Lee, M.D. Ediger, J.J. de Pablo, Heterogeneous dynamics during deformation of a polymer glass, Soft. Matter. 6 (2010) 287–291, https://doi.org/10.1039/B912288E.
[90] T. Wang, Y. Chen, B. Chen, M.J. Suazo, N.S. Purwanto, J.M. Torkelson, Reprocessable, self-healing, and creep-resistant covalent adaptable network made from chain-growth monomers with dynamic covalent thionourethane and disulfide cross-links, ACS. Macro Lett. 13 (2024) 1147–1155, https://doi.org/10.1021/acsmacrolett.4c00391.
[91] R. Chen, L. Zhou, K. Zhang, M. Chen, Adjusting the dynamic and mechanochromic properties of aromatic disulfide epoxy vitrimers by unsaturation of epoxy monomers, J. Appl. Polym. Sci. 141 (2024) e55655, https://doi.org/10.1002/app.55655.
[92] C. Wang, H. Xu, Z. Xie, J. Zheng, J. Wu, Extrudable, robust and recyclable bio-based epoxy vitrimer via tailoring the topology of a dual dynamic-covalent-bond network, Polym. (Guildf) 289 (2023) 126487, https://doi.org/10.1016/j.polymer.2023.126487.
[93] H. Fang, W. Ye, Y. Ding, H.H. Winter, Rheology of the critical transition State of an Epoxy vitrimer, Macromolecules. 53 (2020) 4855–4862, https://doi.org/10.1021/acs.macromol.0c00843.
[94] F. Meng, M.O. Saed, E.M. Terentjev, Rheology of vitrimers, Nat. Commun. 13 (2022) 5753, https://doi.org/10.1038/s41467-022-33321-w.
[95] A. Klingler, J.K. Krüger. Vitrimers: New types of reshapable, repairable, and recyclable polymer matrices - A physical–technical perspective, Multifunctionality of Polymer Composites, William Andrew Publishing, 2026, pp. 1041–1076, https://doi.org/10.1016/B978-0-443-28872-2.00015-2.
[96] L. Yin, Y. Xiao, Q.-W. Li, Y. Tian, C.-M. Shu, Temperature effect on thermal conductivity of oxidised coal associated with its predictive model during coal pyrolysis, Energy 274 (2023) 127417, https://doi.org/10.1016/j.energy.2023.127417.